

Resonance-enhanced high-harmonic generation and attosecond transient absorption spectroscopy of hydrogen atoms

Yue Cao(曹玥), Zheng Shu(舒正), Da-Wei Tian(田大纬), and Xiao-Lei Hao(郝小雷)
Citation: Chin. Phys. B, 2026, 35 (**6**): 064210. DOI: 10.1088/1674-1056/ae64cd
http://cpb.iphy.ac.cn; http://iopscience.iop.org/cpb

What follows is a list of articles you may be interested in

Role of trajectory symmetry in solid high-order harmonic generation

Shuang Wang(王爽), Yu Zhao(赵宇), Hui-Rong Wang(王慧荣), Yun-He Xing(邢云鹤), Xiao-Xin Huo(霍晓鑫), and Jun Zhang(张军)
Chin. Phys. B, 2026, 35 (**4**): 044204. DOI: 10.1088/1674-1056/ae04da

Charge-imbalance-induced second harmonic generation in twisted graphene

Ronghui Luo(罗荣辉), Shiyang Liu(刘诗洋), Xiao Dong(董校), Jianguo Tian(田建国), and Zhibo Liu(刘智波)
Chin. Phys. B, 2026, 35 (**3**): 034201. DOI: 10.1088/1674-1056/ae3557

Optical temporal interference model for investigation and manipulation of non-integer high-order harmonic generation

Zhao-Yue Meng(孟昭越), Yun Pan(潘云), Jun-Ping Wang(王军平), and Xi Zhao(赵曦)
Chin. Phys. B, 2026, 35 (**2**): 024208. DOI: 10.1088/1674-1056/adfdc5

Twin pulses of THz generation from a nonlinear crystalline quartz by femtosecond laser pulse

Xiangmei Dong(董祥美), Dan-Ni Li(李丹妮), Zuan-Ming Jin(金钻明), Hui-Ping Zhang(张慧萍), Hong-Guang Li(李宏光), Shao-Hui Wu(吴少晖), Yan Peng(彭滟), Yiming Zhu(朱亦鸣), and Songlin Zhuang(庄松林)
Chin. Phys. B, 2025, 34 (**9**): 094211. DOI: 10.1088/1674-1056/addbcd

3D-GTDSE: A GPU-based code for solving 3D-TDSE in Cartesian coordinates

Ke Peng(彭科), Aihua Liu(刘爱华), Jun Wang(王俊), and Xi Zhao(赵曦)
Chin. Phys. B, 2025, 34 (**9**): 094203. DOI: 10.1088/1674-1056/adee00

SPECIAL TOPIC — Ultrafast physics in atomic, molecular and optical systems

Resonance-enhanced high-harmonic generation and attosecond transient absorption spectroscopy of hydrogen atoms

Yue Cao(曹玥), Zheng Shu(舒正)†, Da-Wei Tian(田大纬), and Xiao-Lei Hao(郝小雷)

State Key Laboratory of Quantum Optics Technologies and Devices, Institute of Theoretical Physics, Shanxi University, Taiyuan 030006, *China*

(Received 29 December 2025; revised manuscript received 16 April 2026; accepted manuscript online 27 April 2026)

Using *ab initio* simulations, we investigate high-harmonic generation in hydrogen atoms driven by a near-infrared (NIR) laser pulse combined with an attosecond extreme-ultraviolet (XUV) pulse. The efficiency of high-harmonic generation is significantly enhanced when the XUV pulse excites atoms from the ground state to an excited p state. Furthermore, by varying the time delay between the two laser pulses, we calculate the attosecond transient absorption spectra of hydrogen atoms based on numerical solutions of the time-dependent Schrödinger equation (TDSE). Combining attosecond transient absorption spectra with high-harmonic spectra provides a powerful approach for revealing laser-induced energy-level shifts and the splitting structure of resonant harmonic emission.

Keywords: resonance harmonic emission, ac Stark effect, attosecond transient absorption spectra

PACS: 42.65.Ky, 33.20.Xx

DOI: 10.1088/1674-1056/ae64cd **CSTR:** 32038.14.CPB.ae64cd

1. Introduction

High-harmonic generation (HHG) spectroscopy has proven to be a powerful technique for probing ultrafast electron dynamics in laser–matter interactions, offering sub-Å spatial and sub-femtosecond temporal resolution.[1–6] Moreover, HHG serves as an important source for generating extreme-ultraviolet (XUV) radiation.[7–13] The physical mechanism of HHG in gases is well described by the semiclassical three-step model:[14,15] first, a bound electron tunnels through the Coulomb potential barrier and is released as a free-electron wave packet; second, it is accelerated by the laser field; and finally, upon recombination with the parent ion, an XUV photon is emitted.

Resonance-enhanced HHG provides an effective means to improve harmonic conversion efficiency.[16–19] During laser–atom interactions, resonant excitation populates atomic excited states, thereby opening new channels for HHG.[20] These excited states can either emit XUV radiation through free-induction decay or contribute to HHG via ionization from an excited state followed by recombination to the ground state.[21] Below the ionization threshold, bound–bound resonances can significantly enhance resonant harmonic emission.[22–25] When an isolated attosecond pulse excites an electron from the ground state into various excited states, the subsequent interaction with a near-infrared (NIR) laser pulse can generate dressed states, leading to finer spectral structures and enhanced HHG conversion efficiency.

Attosecond transient absorption spectroscopy (ATAS) provides a complementary approach for measuring sub-cycle variations in electronic energy levels induced by a moderately strong NIR field ($\sim 10^{12}$ W/cm^2).[26–29] When the XUV and NIR pulses overlap in time, laser-induced population transfer from the ground state to excited states gives rise to new spectral features below the ionization threshold.[30–36] The time delay between the XUV and NIR pulses provides an additional control parameter for probing dynamical ac Stark shifts[37,38] and Autler–Townes splitting[39,40] induced by the NIR field.

While previous studies have demonstrated resonance-enhanced HHG through excited-state participation, they have largely focused on enhancing the harmonic yield itself. The transient evolution of the resonant states under the influence of the dressing field and its direct impact on the harmonic structure remain to be fully resolved. In this work, we integrate HHG with ATAS to address this gap. The time-resolved nature of ATAS allows us to map the dynamical ac Stark shift and splitting of the resonant level as a function of the XUV–NIR delay, thereby establishing a direct connection between transient modifications of the atomic energy levels and the observed fine structure in the harmonic spectra.

In this work, we investigate resonance-enhanced HHG in hydrogen atoms driven by a NIR field combined with an attosecond XUV pulse through numerical simulations of the three-dimensional time-dependent Schrödinger equation (TDSE). The one-photon 1s–2p resonance induced by the XUV leads to a pronounced enhancement of the harmonic conversion efficiency and, more importantly, a distinct splitting of the resonant harmonic emission is observed in the HHG spectra. By varying the time delay between the XUV and

†Corresponding author. E-mail: zheng_shu@sxu.edu.cn

© 2026 Chinese Physical Society and IOP Publishing Ltd. All rights, including for text and data mining, AI training, and similar technologies, are reserved.

NIR pulses, we observe corresponding changes in the intensity and splitting structure of the resonant harmonics. A combined analysis with attosecond transient absorption spectra demonstrates that the observed spectral splitting arises from the dynamical ac-Stark shift.

This paper is organized as follows. Section 2 provides a brief introduction to the numerical solution of the three-dimensional TDSE and the method used to calculate the attosecond transient absorption spectra. In Section 3, we discuss HHG and attosecond transient absorption spectra under different laser parameters and analyze the mechanism responsible for the resonance-induced harmonic splitting. Finally, Section 4 summarizes our conclusions. Atomic units (a.u.) ($e=\hbar=m_{\rm e}=1$) are used throughout, unless indicated otherwise.

2. Theoretical methods

2.1. The numerical solution of the TDSE and the harmonic spectra

Within the single-active-electron approximation, the TDSE in the length gauge for an atom (in spherical coordinates) is given by[41]

$$\mathrm{i}\frac{\partial}{\partial t}\psi(\boldsymbol{r},t) = \left\{-\frac{1}{2r^2}\frac{\partial}{\partial r}r^2\frac{\partial}{\partial r}+\frac{1}{2r^2}\left[\frac{\partial}{\partial\xi}(1-\xi^2)\frac{\partial}{\partial\xi}-\frac{m^2}{1-\xi^2}\right]+V(\boldsymbol{r})-\boldsymbol{E}(t)\cdot\boldsymbol{r}\right\}\psi(\boldsymbol{r},t), \quad (1)$$

where $\xi=\cos\theta$, and m is the z component of the electronic orbital angular momentum. Here, $V(\boldsymbol{r})=-1/\boldsymbol{r}$ is the Coulomb potential of the hydrogen atom, and $-\boldsymbol{E}(t)\cdot\boldsymbol{r}$ describes the electric-dipole interaction between the atom and the time-dependent external electric field $\boldsymbol{E}(t)$.

The wave function $\psi(\boldsymbol{r},t)$ is expanded in terms of B-splines as follows:

$$\psi(r,t,\xi,\phi)=\frac{1}{\sqrt{2\pi}}\sum_{\mu\nu}C_{\mu\nu}(t)\frac{B_\mu^k(r)}{r}(1-\xi^2)^{\frac{|m|}{2}}B_\nu^k(\xi)\,\mathrm{e}^{\mathrm{i}m\phi}, \quad (2)$$

where $B_\mu^k(r)$ denotes a B-spline basis function of order $k=7$. For the ground state of hydrogen, the magnetic quantum number m is zero. In our calculations, 500 radial B-spline functions and 36 angular basis functions are employed. The maximum radial coordinate $r_{\max}$ is 150 a.u. To suppress unphysical reflections, a $\cos^{1/8}$ absorber function is applied in the region from 100 a.u. to $r_{\max}$.

The NIR and XUV pulses are both polarized along the z-axis and have sine-squared envelopes of the form

$$E(t)=E_0\sin^2\left(\frac{\pi t}{\tau}\right)\sin(\omega t), \quad (3)$$

where E_0 is the peak electric-field amplitude and τ is the pulse duration. The XUV pulse has an intensity of 1×10^{10} W/cm^2, a central wavelength of 120 nm, and a duration of 10 optical cycles. The corresponding photon energy is 10.33 eV, which is resonant with the hydrogen 1s–2p transition. This resonance serves as a prerequisite for resonance-enhanced harmonic emission. The NIR pulse has an intensity of 1×10^{13} W/cm^2, a wavelength of 800 nm, and a duration of 12 optical cycles. The time delay $\tau_{\rm d}$ is defined as the difference between the maxima of the XUV and NIR pulse envelopes. A positive (negative) time delay indicates that the XUV pulse arrives after (before) the NIR pulse.

With the time-dependent wave function $\psi(\boldsymbol{r},t)$, we calculate the induced dipole moment as follows:

$$d(t)=\langle\psi(t)|z|\psi(t)\rangle. \quad (4)$$

The HHG power spectrum is obtained from the Fourier transform

$$P(\omega)=\left|\int\ddot{d}(t)\,\mathrm{e}^{-\mathrm{i}\omega t}\,\mathrm{d}t\right|^2, \quad (5)$$

where $\ddot{d}(t)=\frac{\mathrm{d}^2}{\mathrm{d}t^2}\langle\psi(t)|z|\psi(t)\rangle$ is the time-dependent dipole acceleration.

The populations of the excited states are calculated by projecting the total wave function onto the eigenstates of the hydrogen atom[42]

$$|c_k(t)|^2=\left|\int_{-\infty}^{\infty}\phi_k^*(\boldsymbol{r})\psi(\boldsymbol{r},t)\,\mathrm{d}\boldsymbol{r}\right|^2, \quad (6)$$

where $\phi_k^*(\boldsymbol{r})$ is the complex conjugate of the hydrogenic eigenstate wave function.

We further decompose the time-dependent wave function into bound-state components (from 1s to 4f) and a continuum component

$$|\phi(t)\rangle=\sum_{k\in\mathcal{B}}c_k(t)|\phi_k\rangle+|\phi_c(t)\rangle, \quad (7)$$

where $\mathcal{B}=\{1\mathrm{s},2\mathrm{s},2\mathrm{p},3\mathrm{s},3\mathrm{p},3\mathrm{d},4\mathrm{s},4\mathrm{p},4\mathrm{d},4\mathrm{f}\}$ and $|\phi_c(t)\rangle$ denote the continuum component. The continuum-to-bound recombination contribution is defined as

$$d_{k\text{-}continuum}(t)\equiv c_k^*(t)\langle\phi_k|z|\psi_c(t)\rangle+\mathrm{c.c.}, \quad (8)$$

while the bound-to-bound recombination contribution is defined as

$$d_{k\text{–}m}(t)\equiv c_k^*(t)c_m(t)\langle\phi_k|z|\phi_m\rangle+\mathrm{c.c.} \quad (9)$$

2.2. The calculation of the attosecond transient absorption spectra

In theory, laser-dressed absorption can be described within a semiclassical framework, in which a quantum atom is driven by a classical electromagnetic field.[30] The attosecond

transient absorption spectra are related to the response function defined as[43]

$$S(\omega,\tau_{\rm d}) = -\frac{2\omega}{\tau_{\rm NIR}-\tau_{\rm d}}{\rm Im}\left[\tilde{d}(\omega,\tau_{\rm d})\tilde{E}^{*}(\omega,\tau_{\rm d})\right], \quad (10)$$

where $\tilde{d}(\omega,\tau_{\rm d})$ is the Fourier transform of the dipole moment along the laser polarization axis, and $\tilde{E}^{*}(\omega,\tau_{\rm d})$ is the Fourier transform of the driving laser field. $\tau_{\rm NIR}$ and $\tau_{\rm d}$ denote the duration of the NIR pulse and the time delay between the NIR and XUV pulses, respectively. When $S(\omega,\tau_{\rm d})$ is positive, the atom predominantly absorbs radiation at that frequency, whereas when $S(\omega,\tau_{\rm d})$ is negative, the atom predominantly emits radiation at that frequency. The corresponding absorption cross section is given by

$$\sigma(\omega,\tau_{\rm d}) = \frac{4\pi\alpha\omega S(\omega,\tau_{\rm d})}{|\tilde{E}(\omega,\tau_{\rm d})|^{2}}, \quad (11)$$

where α is the fine-structure constant ($\alpha \approx 1/137$). Experimental measurements of transient absorption spectra are typically based on Beer's law, which relates the transmitted light intensity to the absorption cross section, interaction length, and medium density. Using Beer's law,[30] the attosecond transient absorption spectra can be calculated as

$$e^{-\sigma(\omega,\tau_{\rm d})L/2}, \quad (12)$$

where L denotes the interaction length. In our calculations, $L = 2$, which provides a reasonable approximation to experimental conditions.[43]

3. Results and discussion

In this study, we focus on the one-photon resonance between the XUV pulse and the hydrogen 1s–2p transition. Figure 1 shows the XUV pulse (red solid line) and NIR pulse (black dashed line) with $\tau_{\rm d} = -5T_{\rm NIR}$, where $T_{\rm NIR}$ is the optical cycle of the NIR pulse.

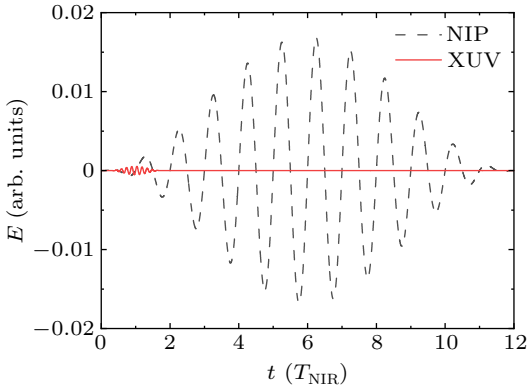


Fig. 1. Temporal profiles of the XUV pulse (red solid line) and the NIR pulse (black dashed line). The time delay $\tau_{\rm d}$ is defined as the difference between the maxima of the XUV and NIR pulse envelopes and is set to $-5T_{\rm NIR}$.

Figure 2(a) presents the high-harmonic spectra of the hydrogen atom driven solely by the NIR pulse (black dashed line) at an intensity of 1×10^{13} W/cm^2 and by a two-color laser field (red solid line) consisting of the NIR and XUV pulses. The XUV pulse has an intensity of 1×10^{10} W/cm^2 and is tuned to the one-photon 1s–2p resonance, with a time delay of $-5T_{\rm NIR}$ relative to the NIR pulse. The introduction of this weak XUV pulse, whose intensity is only 0.1% of that of the NIR pulse, results in a pronounced enhancement of the harmonic conversion efficiency.

The vertical line in Fig. 2(a) marks the resonance energy gap between the ground (1s) and excited (2p) states, corresponding to 10.2 eV. Even in the NIR-only case, weak photon emission associated with the 2p–1s transition can be observed (see Fig. 2(b)), although its intensity is extremely low. When the XUV pulse resonantly excites electrons from the 1s state to the 2p state via a one-photon transition, the resonant harmonic emission is enhanced by approximately seven orders of magnitude compared with the NIR-only case.

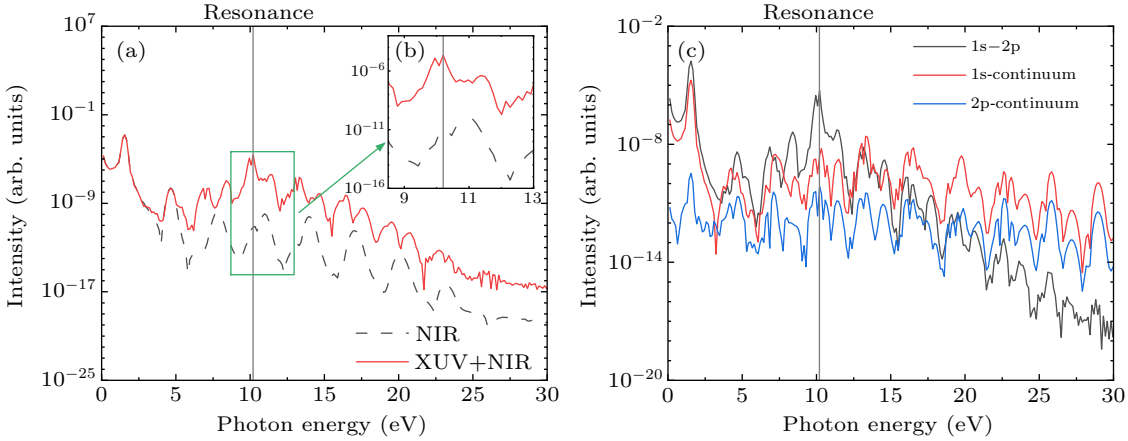


Fig. 2. (a) High-harmonic spectra of the hydrogen atom driven by the NIR pulse alone (black dashed line) and by the combined NIR and XUV fields with a time delay $\tau_{\rm d} = -5T_{\rm NIR}$ (red solid line). (b) Enlarged view of the harmonic spectrum in (a) over the photon-energy range 8.5–13 eV. (c) High-harmonic spectra from different emission channels: contributions from continuum-to-bound recombination into the 1s state (1s–continuum, red line), continuum-to-bound recombination into the 2p state (2p–continuum, blue line), and the 1s–2p bound–bound transition (black line).

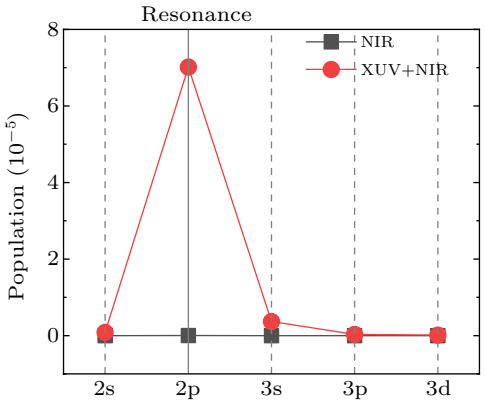


Fig. 3. Populations of the excited states of the hydrogen atom at the end of the laser pulse, for the cases of excitation by the NIR pulse alone (black squares) and by the combined NIR and XUV fields with $\tau_d = -5T_{NIR}$ (red circles).

Figure 3 further compares the excited-state populations obtained with the NIR pulse alone (black squares) and with the two-color laser pulse (red circles). As shown, the population of the 2p state increases by about seven orders of magnitude upon the introduction of the XUV pulse. Therefore, the pronounced enhancement of the harmonic emission near 10.2 eV can be directly attributed to the one-photon resonant excitation induced by the XUV pulse. To reveal the dominant channel and the origin of the resonant feature, we compare high-harmonic spectra from different emission channels. As shown in Fig. 2(c), the 1s–2p transition exhibits a pronounced resonant peak near 10.2 eV, indicating that this feature is closely linked to the 1s–2p transition induced by resonant excitation.

The enhancement of the harmonic emission near 10.2 eV is accompanied by a distinct splitting of the resonant peak. Figure 4(a) compares the high-harmonic spectra obtained with two-color laser fields while varying the XUV intensity at a fixed time delay of $\tau_d = -5T_{NIR}$. It is evident that the intensity of the resonant emission increases with increasing XUV intensity, whereas the positions of the split peaks remain nearly unchanged for different XUV intensities. The integrated intensity of the resonant harmonic emission around 10.2 eV is plotted as a function of the XUV intensity in Fig. 4(b) (black squares).

Figure 4(c) shows the population of the 2p excited state (red circles) as a function of the XUV intensity under a two-color field driving. As observed, the enhancement of the resonant harmonic emission scales proportionally with the population of the 2p state.

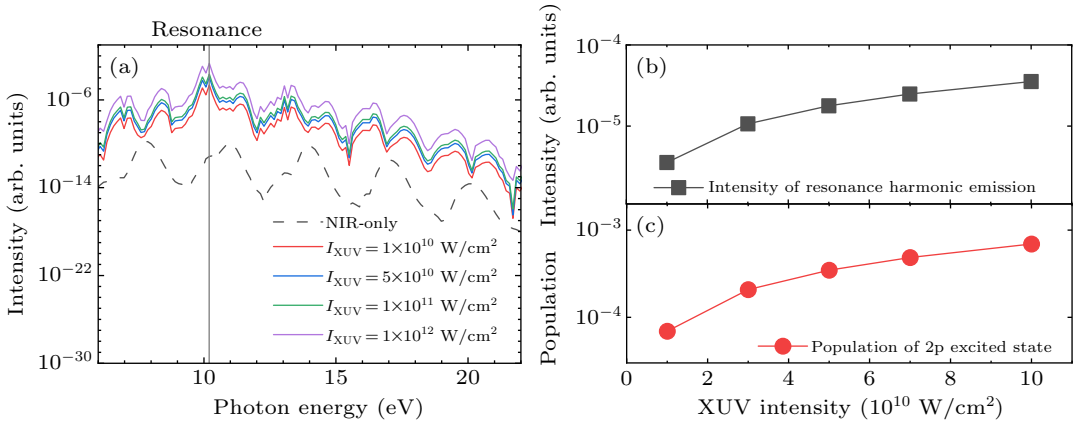


Fig. 4. (a) High-harmonic spectra generated by two-color laser fields with different XUV intensities at a fixed time delay $\tau_d = -5T_{NIR}$. The black dashed line corresponds to the NIR-only case, while the red, blue, green, and purple solid lines represent XUV intensities of 1×10^{10} W/cm^2, 5×10^{10} W/cm^2, 1×10^{11} W/cm^2, and 1×10^{12} W/cm^2, respectively. (b) Integrated intensity of the resonant harmonic emission around 10.2 eV as a function of the XUV intensity. (c) Population of the 2p excited state as a function of the XUV intensity. The time delay is fixed at $\tau_d = -5T_{NIR}$.

Figures 5(a) and 5(b) show the absorption spectra as a function of the XUV and NIR intensities, respectively, calculated according to Eq. (12) at a fixed time delay $\tau_d = -5T_{NIR}$. As seen in Fig. 5(a), the absorption line located at 10.2 eV remains essentially unchanged with varying XUV intensities, indicating that the resonance position is independent of the XUV intensity. We then examine the dependence of the absorption spectra on the NIR intensity, as shown in Fig. 5(b). The most striking feature is that the absorption line near 10.2 eV gradually splits and broadens with increasing NIR intensity. This behavior arises from the laser-induced dynamical ac-Stark shift, which modifies the atomic energy levels in the presence of a strong NIR field.

For the parameters used in this work, the NIR photon energy is 1.55 eV, whereas the 2p–3s transition energy is approximately 1.89 eV. Therefore, the driving-field frequency is smaller than the corresponding transition frequency, corresponding to red detuning rather than blue detuning. Under red detuning, the lower state shifts to lower energy, while the upper state shifts to higher energy.[44] In the present 2p–3s coupling, since 2p is the lower state of the pair, it experiences a downward ac Stark shift under red-detuned driving.

The observed broadening of the 2p level at an NIR intensity of 1×10^{13} W/cm^2 in Fig. 5(b) is approximately 0.3–0.4 eV. We estimate the shift using the generalized dressed-

state expression[45]

$$\Delta E = \sqrt{(\mu E_{\mathrm{NIR}})^2 + \delta^2}, \tag{13}$$

where μ is the relevant dipole matrix element and δ is the detuning. For the NIR intensity used in our simulations ($I_{\mathrm{NIR}} = 1 \times 10^{13}$ W/cm^2), the peak electric-field amplitude is approximately $E_{\mathrm{NIR}} \approx 0.017$ a.u. The dipole matrix element for the 2p–3s transition is 0.542 a.u.[43] Using these values, the estimated energy shift is approximately 0.42 eV, in reasonable agreement with the numerical results obtained from both the HHG and absorption spectra.

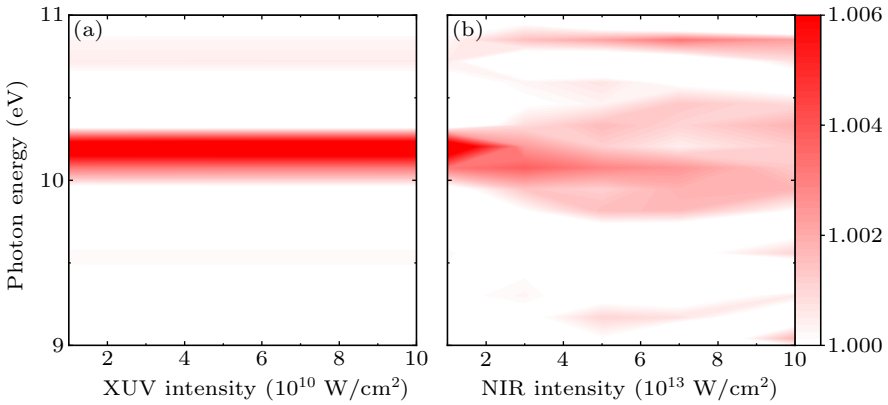


Fig. 5. Calculated absorption spectra of the hydrogen atom as a function of the XUV and NIR intensities. The time delay is fixed at $\tau_{\mathrm{d}} = -5T_{\mathrm{NIR}}$. (a) Absorption spectra as a function of the XUV intensity. The XUV pulse has a wavelength of 120 nm and a duration of 10 optical cycles, while the NIR pulse has an intensity of 1×10^{13} W/cm^2, a wavelength of 800 nm, and a duration of 12 optical cycles. (b) Absorption spectra as a function of the NIR intensity. The XUV pulse has an intensity of 1×10^{10} W/cm^2, a wavelength of 120 nm, and a duration of 10 optical cycles, while the NIR pulse has a wavelength of 800 nm and a duration of 12 optical cycles.

Although a strong NIR field can dress atomic levels and induce a dynamical ac Stark shift during the interaction, the observation of a clearly resolved level shift in the harmonic spectrum requires not only NIR-induced dressing but also a sufficiently strong and coherent radiative pathway to probe the dressed-state structure.

In the present parameter regime (800 nm, 1×10^{13} W/cm^2), the NIR field is far detuned from the 1s–2p one-photon resonance and therefore induces only a weak population transfer to the 2p state. As a result, the emission near 10.2 eV in the NIR-only case is extremely weak and significantly broadened, preventing a reliable resolution of the fine level shift.

In contrast, the weak resonant XUV pulse efficiently prepares population and coherence in the 2p state, strongly enhancing the resonant emission and making the NIR-induced ac Stark shift clearly observable. In this scheme, the NIR field primarily determines the level shift through dynamical dressing, while the XUV pulse acts as a preparation and probe channel that enables the dressed-state structure to be accessed.

This interpretation is consistent with our numerical results, where the splitting positions are nearly independent of the XUV intensity, whereas the apparent level shift becomes more pronounced with increasing NIR intensity.

Furthermore, we compare the high-harmonic spectra obtained at different time delays between the XUV and NIR pulses, as shown in Fig. 6(a). In this comparison, the XUV intensity is 1×10^{10} W/cm^2 and the NIR intensity is 1×10^{13} W/cm^2.

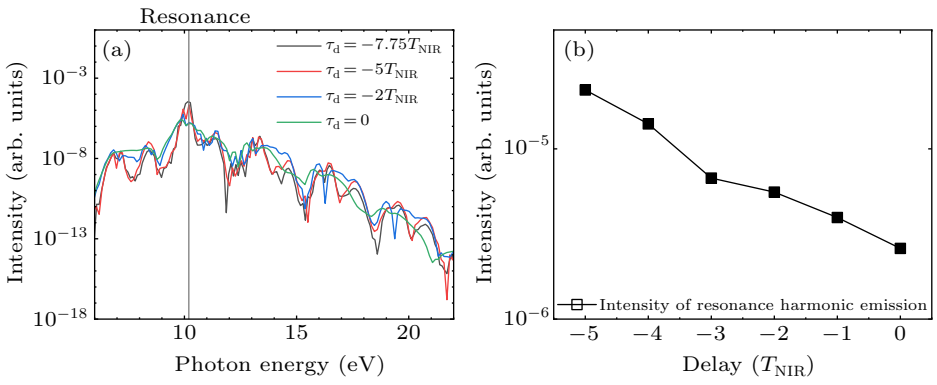


Fig. 6. (a) High-harmonic spectra generated by two-color laser fields at different time delays: $\tau_{\mathrm{d}} = -7.75T_{\mathrm{NIR}}$ (black), $-5T_{\mathrm{NIR}}$ (red), $-2T_{\mathrm{NIR}}$ (blue), and 0 (green). (b) Intensity of the resonant harmonic emission around 10.2 eV as a function of the time delay τ_{d}.

The black line corresponds to the case where the XUV pulse arrives before the NIR pulse with a delay of $\tau_d = -7.75T_{NIR}$; in this case, the two pulses do not overlap in time. The red line corresponds to $\tau_d = -5T_{NIR}$ (see the laser fields in Fig. 1), where the XUV pulse overlaps with the rising edge of the NIR pulse. The green line represents the zero-delay case, where the maxima of the two pulses coincide.

The splitting of the resonant harmonic near 10.2 eV disappears when the pulses are temporally separated (black line in Fig. 6(a)), confirming that the level shift of the 2p state originates from the dynamical ac Stark shift induced by the NIR field. In addition, the emission intensity near 10.2 eV in the zero-delay case (green line) is lower than in the non-overlapping case (black line). This is because, when the two pulses fully overlap, the XUV pulse acts only as a weak probe compared with the much stronger NIR field, leading to reduced resonant emission.

We further extract the resonant harmonic intensity from Fig. 6(a) and present its delay dependence in Fig. 6(b). The results show that the resonant harmonic emission decreases markedly as the time delay is reduced from $-5T_{NIR}$ to 0, i.e., as the XUV pulse approaches the center of the NIR pulse.

To elucidate the underlying mechanism, we further present the time-frequency distribution of the high-harmonic emission driven by the two-color laser field at different time delays. As shown in Fig. 7(a), the case of $\tau_d = -5T_{NIR}$ exhibits a clear temporal distribution of the signal at 10.2 eV. On the rising and falling edges of the NIR pulse, where the instantaneous field strength is relatively weak, the dynamics are dominated by resonant emission associated with the 2p–1s transition. In contrast, near the peak of the NIR pulse envelope, strong-field ionization of the excited 2p state becomes significant, increasing the above-threshold harmonic yield within the three-step strong-field framework.

As shown in Figs. 7, the time delay decreases progressively from panel (a) to panel (f). These time-frequency analyses show that the resonant harmonic signal at 10.2 eV gradually weakens as the time delay decreases. Although the XUV pulse still excites the system at shorter delays, the increasing instantaneous NIR field rapidly ionizes the excited population. This depletion of the 2p state reduces the population available for resonant recombination, thereby suppressing the harmonic emission near 10.2 eV.

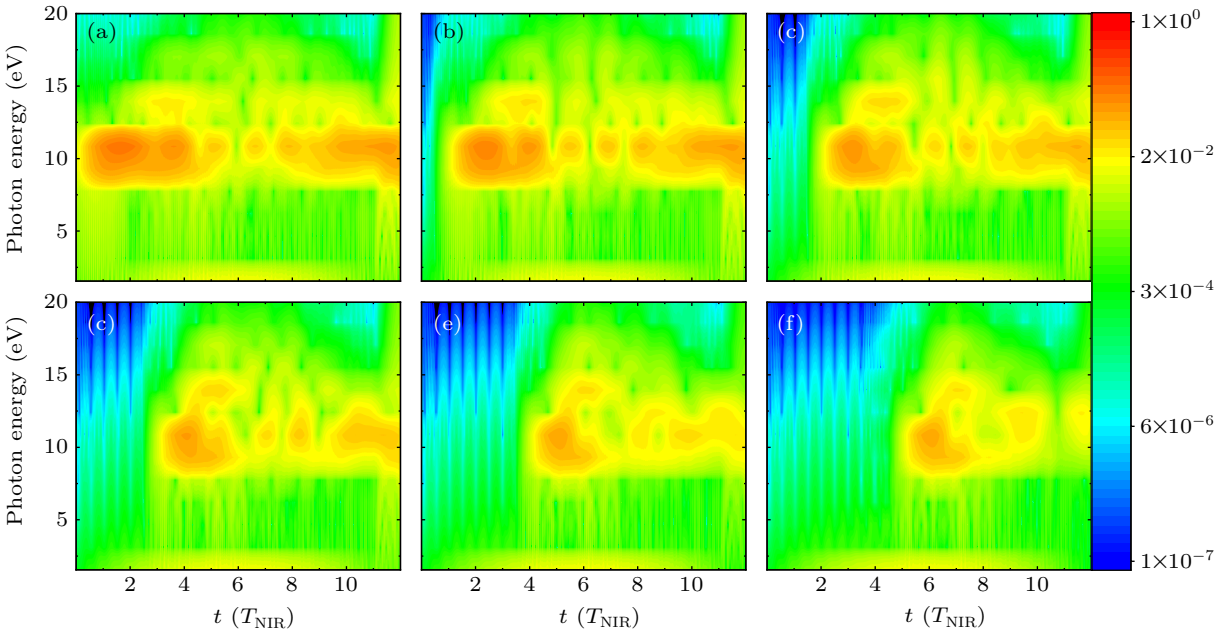


Fig. 7. Time-frequency distributions of high-harmonic emission at different time delays τ_d. The vertical axis denotes the photon energy, the horizontal axis denotes time in units of the NIR optical cycle, and the color scale represents the logarithmic intensity of the harmonic emission. Panels (a)–(f) correspond to time delays of $-5T_{NIR}$, $-4T_{NIR}$, $-3T_{NIR}$, $-2T_{NIR}$, $-T_{NIR}$, and 0, respectively.

The splitting structure of the resonant harmonic should not be interpreted as an instantaneous splitting of a single energy level. Instead, it arises from a temporal superposition of emissions generated at different stages of the laser pulse. On the rising and falling edges of the NIR pulse, where the field intensity is relatively weak, the 2p level remains close to its field-free position and contributes emission near the unperturbed resonance energy. Around the peak of the NIR pulse, however, the stronger field induces a pronounced ac Stark shift of the 2p level.

Since the high-harmonic spectrum is obtained by integrating over the full temporal evolution, these temporally separated contributions are simultaneously mapped into the frequency domain, resulting in a double-peak structure. This mechanism is distinct from Autler–Townes splitting, which typically arises from strong near-resonant coupling between

two states and leads to the formation of dressed states with approximately symmetric energy separation around the field-free level. In contrast, the ac Stark effect considered here originates from off-resonant coupling and primarily induces energy shifts rather than true level splitting.

Figure 8 shows the attosecond transient absorption spectra as a function of the time delay. The absorption line near 10.2 eV becomes narrower as the delay increases. At a larger negative delay of approximately $-6T_{\mathrm{NIR}}$, a new spectral feature emerges around 9.8 eV, which may arise from time-dependent interference between XUV-induced excitation of the 2p state and subsequent dressing dynamics induced by the NIR pulse.

Furthermore, the spectral features associated with the 1s–2p transition are clearly visible at different time delays, providing additional evidence of the level shifts of the NIR-dressed states.

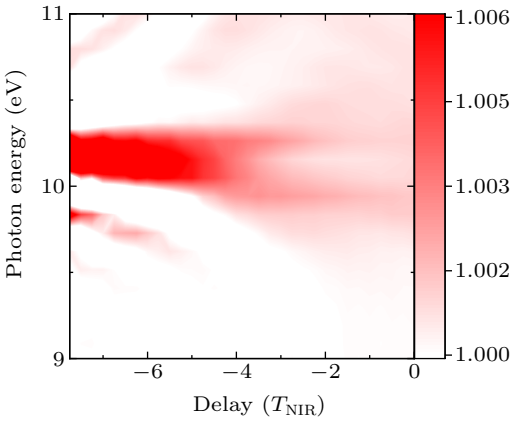


Fig. 8. Calculated attosecond transient absorption spectra as a function of the time delay τ_{d}. The time-delay step is $0.1T_{\mathrm{NIR}}$. The XUV pulse has an intensity of 1×10^{10} W/cm^2, a wavelength of 120 nm, and a duration of 10 optical cycles. The NIR pulse has an intensity of 1×10^{13} W/cm^2, a wavelength of 800 nm, and a duration of 12 optical cycles.

4. Conclusion

In summary, we have investigated resonance-enhanced high-harmonic generation in atomic hydrogen driven by a NIR field combined with a weak, resonant attosecond XUV pulse. Through *ab initio* simulations of the three-dimensional time-dependent Schrödinger equation, we demonstrate that an XUV pulse tuned to the 1s–2p one-photon transition dramatically enhances the harmonic conversion efficiency compared with the NIR-only case. This enhancement is directly linked to XUV-induced population and coherence in the 2p excited state.

Furthermore, we observe a pronounced splitting of the resonant harmonic emission near 10.2 eV. By systematically varying the time delay between the XUV and NIR pulses and analyzing the corresponding attosecond transient absorption spectra, we attribute this splitting to a temporal superposition of emissions generated at different stages of the laser pulse. The splitting emerges only when the two pulses overlap temporally, confirming its origin in laser-dressed atomic dynamics.

The combined analysis of high-harmonic generation and attosecond transient absorption spectroscopy provides a powerful approach for probing laser-induced level shifts with high spectral and temporal resolution. This framework may be extended to molecular systems in future studies.

Acknowledgment

This work was supported by the National Natural Science Foundation of China (Grant Nos. 12304304 and 12274273).

References

[1] Bruner B D, Mašín Z, Negro M, Morales F, Brambila D, Devetta M, Faccialà D, Harvey A G, Ivanov M, Mairesse Y, Patchkovskii S, Serbinenko V, Soifer H, Stagira S, Vozzi C, Dudovich N and Smirnova O 2016 *Faraday Discuss.* **194** 369
[2] He L X, Sun S Q, Lan P F, He Y Q, Wang B C, Wang P, Zhu X S, Li L, Cao W, Lu P X and Lin C D 2022 *Nat. Commun.* **13** 4595
[3] Marangos J P, Baker S, Kajumba N, Robinson J S, Tisch J W G and Torres R 2008 *Phys. Chem. Chem. Phys.* **10** 35
[4] Cireasa R, Boguslavskiy A E, Pons B, Wong M C H, Descamps D, Petit S, Ruf H, Thiré N, Ferré A, Suarez J, Higuet J, Schmidt B E, Alharbi A F, Légaré F, Blanchet V, Fabre B, Patchkovskii S, Smirnova O, Mairesse Y and Bhardwaj V R 2015 *Nat. Phys.* **11** 654
[5] Jiménez Á, Zhavoronkov N, Schloz M, Morales F and Ivanov M 2017 *Opt. Express* **25** 22880
[6] Bauer M 2005 *J. Phys. D: Appl. Phys.* **38** R253
[7] Spielmann C, Burnett N H, Sartania S, Koppitsch R, Schnürer M, Kan C, Lenzner M, Wobrauschek P and Krausz F 1997 *Science* **278** 661
[8] Chang Z H, Rundquist A, Wang H W, Murnane M M and Kapteyn H C 1997 *Phys. Rev. Lett.* **79** 2967
[9] Schnürer M, Spielmann C, Wobrauschek P, Streli C, Burnett N H, Kan C, Ferencz K, Koppitsch R, Cheng Z, Brabec T and Krausz F 1998 *Phys. Rev. Lett.* **80** 3236
[10] Xiong H, Xu H, Fu Y X, Yao J, Zeng B, Chu W, Cheng Y, Xu Z Z, Takahashi E J, Midorikawa K, Liu X and Chen J 2009 *Opt. Lett.* **34** 1747
[11] Chen M C, Arpin P, Popmintchev T, Gerrity M, Zhang B, Seaberg M, Popmintchev D, Murnane M M and Kapteyn H C 2010 *Phys. Rev. Lett.* **105** 173901
[12] Popmintchev T, Chen M C, Popmintchev D, Arpin P, Brown S, Ališauskas S, Andriukaitis G, Balčiunas T, Mücke O, Pugzlys A, Baltuška A, Shim B, Schrauth S E, Gaeta A, Hernández G C, Plaja L, Becker A, Jaron B A, Murnane M M and Kapteyn H C 2012 *Science* **336** 1287
[13] Du L L, Bu J Y, Chen C B and Zhou X X 2025 *Chin. Phys. B* **34** 123301
[14] Krause J L, Schafer K J and Kulander K C 1992 *Phys. Rev. Lett.* **68** 3535
[15] Corkum P B 1993 *Phys. Rev. Lett.* **71** 1994
[16] Toma E S, Antoine P, Bohan A D and Muller H G 1999 *J. Phys. B: At. Mol. Opt. Phys.* **32** 5843
[17] Zeng Z N, Li R X, Cheng Y, Yu W and Xu Z Z 2002 *Phys. Scr.* **66** 321
[18] Ganeev R A and Redkin P V 2008 *Opt. Commun.* **281** 4126
[19] Haessler S, Strelkov V, Elouga Bom L B, Khokhlova M, Gobert O, Hergott J F, Lepetit F, Perdrix M, Ozaki T and Sali'eres P 2013 *New J. Phys.* **15** 013051
[20] Bian X B and Bandrauk A D 2010 *Phys. Rev. Lett.* **105** 093903
[21] Beaulieu S, Camp S, Descamps D, Comby A, Wanie V, Petit S, Légaré F, Schafer K J, Gaarde M B, Catoire F and Mairesse Y 2016 *Phys. Rev. Lett.* **117** 203001
[22] Fareed M A, Strelkov V V, Thiré N, Mondal S, Schmidt B E, Légaré F and Ozaki T 2017 *Nat. Commun.* **8** 16061
[23] Khokhlova M A, Emelin M Y, Ryabikin M Y and Strelkov V V 2021 *Phys. Rev. A* **103** 043114
[24] Lai Y H, Rao K S, Liang J G, Wang X, Guo C L, Yu W L and Li W 2021 *Opt. Lett.* **46** 2372

[25] Xing Y H, Zhang J, He M L, Huo X X, Wang S, Li Z A and Liu X S 2024 *Phys. Rev. A* **110** 023118
[26] Gaarde M B, Buth C, Tate J L and Schafer K J 2011 *Phys. Rev. A* **83** 013419
[27] Liu Z Y, Cavaletto S M, Ott C, Meyer K, Mi Y H, Harman Z, Keitel C H and Pfeifer T 2015 *Phys. Rev. Lett.* **115** 033003
[28] Fu Y, Xu F and Jin C 2025 *Chin. Phys. B* **34** 063302
[29] Wang X H, Zhao D and Li P B 2025 *Chin. Phys. B* **34** 113201
[30] Chini M, Zhao B Z, Wang H, Cheng Y, Hu S X and Chang Z H 2012 *Phys. Rev. Lett.* **109** 073601
[31] Chu W C and Lin C D 2012 *Phys. Rev. A* **85** 013409
[32] Tarana M and Greene C H 2012 *Phys. Rev. A* **85** 013411
[33] Chen S H, Wu M X, Gaarde M B and Schafer K J 2013 *Phys. Rev. A* **87** 033408
[34] Wu M X, Chen S H, Gaarde M B and Schafer K J 2013 *Phys. Rev. A* **88** 043416
[35] Chini M, Wang X W, Cheng Y and Chang Z H 2014 *J. Phys. B: At. Mol. Opt. Phys.* **47** 124009
[36] Yang Z Q, Ye D F, Ding T, Pfeifer T and Fu L B 2015 *Phys. Rev. A* **91** 013414
[37] Fedorov M V and Movsesian A M 1989 *J. Opt. Soc. Am. B* **6** 1504
[38] Xu X, Qing B, Chen X Z and Zhou X J 2015 *Phys. Lett. A* **379** 1347
[39] Li W K, Wang Y X, Li X, Yang T, Zhang D D and Ding D J 2025 *Phys. Rev. A* **111** 063102
[40] Wu L L, Jiang W C and Peng L Y 2024 *Chin. Phys. B* **33** 074204
[41] Lv H, Zuo W L, Zhao L, Xu H F, Jin M X, Ding D J, Hu S L and Chen J 2016 *Phys. Rev. A* **93** 033415
[42] Fang Y, Tian D W, Cao Y, Hao X L and Shu Z 2025 *Chin. Phys. B* **34** 103201
[43] Murakami M and Chu S I 2013 *Phys. Rev. A* **88** 043428
[44] Bordé C J, Camy G and Decomps B 1979 *Phys. Rev. A* **20** 254
[45] Richter F, Saalmann U, Allaria E, *et al.* 2024 *Nature* **636** 337